INTERNATIONAL JOURNAL OF CLIMATOLOGY
Int. J. Climatol. **27**: 1421–1438 (2007)
Published online 1 February 2007 in Wiley InterScience
(www.interscience.wiley.com) DOI: 10.1002/joc.1482

RMetS
ROYAL METEOROLOGICAL SOCIETY

Basin-wide warming of the Indian Ocean during El Niño and Indian Ocean dipole years

J. S. Chowdary and C. Gnanaseelan*
Indian Institute of Tropical Meteorology, Pune – 411 008, India

Abstract:

Basin-wide wintertime surface warming is observed in the Indian Ocean during El Niño years. The basin-wide warming is found to be stronger when El Niño and Indian Ocean Dipole (IOD) co-occur. The mechanisms responsible for the basin-wide warming are different for the years with El Niño only (El Niño without IOD) and for the co-occurrence (both El Niño and IOD) years. Strong westward propagation of downwelling Rossby waves is observed in the southern Indian Ocean during the IOD years. Such strong propagation is not seen in the case of the El Niño-only years. This indicates that the ocean dynamics play an important role in winter warming of the western Indian Ocean during the IOD years. The weak easterly wind anomalies in the El Niño-only years show no measurable impact on the Wyrtki Jets, but weakening or reversal of these jets is seen in the IOD years. This strongly suggests that the variability related to surface circulation is due to the local IOD forcing rather than El Niño induced wind anomaly. For the El Niño-only composites, surface heat fluxes (mainly latent heat flux and short wave radiation) play an important role in maintaining the basin-wide surface warming in the Indian Ocean. In the IOD-only composites (when there is no El Niño in the Pacific), such basin-wide warming is not seen because of the absence of ENSO (El Niño and Southern Oscillation) induced subsidence over the eastern Indian Ocean. For the years in which both El Niño in the Pacific and dipole in the Indian Ocean co-occur, warming in the western Indian Ocean is due to the ocean dynamics and that in the eastern Indian Ocean is due to the anomalous latent heat flux and solar radiation. Copyright © 2007 Royal Meteorological Society

KEY WORDS basin-wide warming; Indian Ocean Dipole; El Niño

Received 17 May 2005; Revised 14 November 2006; Accepted 19 November 2006

INTRODUCTION

The interannual Sea Surface Temperature (SST) variability in the Indian Ocean is mainly influenced by the tropical ocean–atmospheric interactions such as El Niño, which in fact influences the Indian Ocean through the atmospheric tele-connections associated with the southern oscillation (Bjerknes, 1969). The warming events in the Indian Ocean appear to be a near mirror image of the warming events in the Pacific (Chambers *et al*., 1999). According to Tourre and White (1997) and Nicholson (1997), the atmospheric effects that drive the El Niño in the Pacific Ocean cause similar interannual warming anomalies in the tropical Indian Ocean. During the La Nina years the Indian Ocean experienced basin-wide cooling during the winter due to the propagation of upwelling Rossby waves (Chowdary *et al*., 2006). However, recently it has been observed that the warming (cooling) in the western Indian Ocean (eastern Indian Ocean) takes place during the Indian Ocean Dipole (IOD) years (Saji *et al*., 1999; Webster *et al*., 1999) even in the absence of El Niño (La Nina). The IOD events are characterized by the anomalous cooling in the southeastern equatorial Indian Ocean and anomalous warm SSTs in the western Indian Ocean (Saji *et al*., 1999; Webster *et al*., 1999).

On several occasions, both El Niño in the Pacific Ocean and IOD in the Indian Ocean co-occurred, but on many occasions IOD occurred during non El Niño years. Rao *et al*. (2002) found that, of the 127 years they studied, 65% of the strong IOD events occurred when there was no El Niño in the Pacific and the remaining 35% co-occurred with El Niño and Southern Oscillation (ENSO). During the IOD years, initially cool SST anomalies develop along the Sumatra-Java coast in the eastern equatorial Indian Ocean in May/June. Easterly wind anomalies over the east equatorial Indian Ocean (westerly in the normal years) get strengthened during the mid monsoon months. These strong wind anomalies enhance upwelling in the Sumatra coast and cause further cooling over that region. By October–November the peak phase of the dipole mode occurs with strong east–west gradients in the SST along the equator. The transport of warm water from eastern equatorial Indian Ocean to western Indian Ocean changes the climatic conditions around the Indian Oceanic rim. Normal convective activities over the eastern equatorial Indian Ocean shift to the zones of warm waters in the western Indian

* Correspondence to: C. Gnanaseelan, Indian Institute of Tropical Meteorology, Pune – 411 008, India. E-mail: seelan@tropmet.res.in

Ocean, resulting in drought conditions in Indonesia and floods in East Africa (Saji *et al*., 1999; Webster *et al*., 1999).

Several studies have been already carried out to explain the physical processes associated with the eastern cooling and the western warming during IOD years. Specifically, there have been debates on the mechanisms responsible for warming of the western Indian Ocean. For example, Saji *et al*. (1999) and Murtugudde *et al*. (2000) suggested that western warming is initiated by weak summer monsoon winds and its associated internal dynamics in terms of downwelling Rossby waves. Yu and Reinecker (1999) suggested that the warming is due to the changes in the latent heat flux induced by wind speed. Webster *et al*. (1999) pointed out the role of ocean dynamics in warming the ocean and Prasad and McClean (2004) recently emphasized the importance of the southern Arabian Sea and the local changes in the monsoonal winds for warming of the western Indian Ocean. The eastern cooling is found to have been caused by coastal upwelling (Saji *et al*., 1999; Webster *et al*., 1999; Murtugudde *et al*., 2000; Vinayachandran *et al*., 2002).

Previous studies were carried out mainly to understand the anomalous heating (cooling) of the Indian Ocean in the interannual timescale. However, understanding the mechanisms responsible for warming in the entire Indian Ocean following El Niño in the Pacific is very important as it has several impacts on the climate over this region. In the present study, the mechanisms responsible for the basin-wide warming of the Indian Ocean in the boreal winter (both at the surface and subsurface) are examined using different data sets. It is emphasized that the warming mechanisms during the years when El Niño co-occur with IOD are different from the El Niño-only (no IOD) years. Though Tokinaga and Tanimoto (2004) recently addressed some of the questions related to basin-wide warming focusing on ENSO (El Niño Southern Oscillation) induced subsidence over the Indian Ocean, questions such as whether the same mechanism is responsible for warming in the El Niño-only years and co-occurrence years were not answered. Also, it is important to examine how subsurface anomalies respond to the surface warming over the Indian Ocean. It is shown that during the El Niño-only years the ocean dynamics play a negligible role in the surface and subsurface variability, whereas the internal ocean dynamics play a major role (than the remote forcing) in the variability during the IOD years. We have also brought out the importance of local ocean–atmospheric interaction (air–sea coupling) in influencing the surface circulation over the Indian Ocean. The following section gives a brief description about the data sets, and the next section presents the results and discussion, focusing more on the different mechanisms responsible for basin-wide warming during the El Niño-only years and the co-occurrence years, and the conclusions are presented in the last section.

DATA

Hadley center Ice Sea-Surface Temperature (HadISST) v.1.1 data (Rayner *et al*., 2003) has been used to examine the basin-wide surface warming in the Indian Ocean. The Simple Ocean Data Assimilation (SODA) subsurface temperatures, currents and Sea-Surface Height (SSH) (Carton *et al*., 2000) are also extensively used in the study. The heat content of the upper 250 m is computed on the basis of the SODA temperature profiles. The assimilation product used for SODA is based on the Geophysical Fluid Dynamics Laboratory ocean model, Modular Ocean Model (MOM) 2.2. Surface heat fluxes used in the analysis are from the National Center for Environmental Prediction-National Center for Atmospheric Research (NCEP-NCAR) reanalysis product (Kalnay *et al*., 1996) and Comprehensive Ocean–Atmosphere Data set (COADS) (Woodruff *et al*., 1998), and the surface winds are from NCEP-NCAR. The study period is 52 years (from 1950 to 2001), which covers most of the recent El Niño in the Pacific and dipole mode events in the Indian Ocean. Anomalies of all the fields are calculated on the basis of the 52-year mean.

RESULTS AND DISCUSSIONS

Throughout the paper, the year in which El Niño peaks and the following year are designated, respectively, by (0) and (1). The Niño 3.4 index is prepared from the HadISST anomaly by averaging it over the region 5°N to 5°S and 170°W to 120°W (Trenberth, 1997). This time series is further smoothed with a 5-month running mean and removing the linear trend over the 52-year period. The Niño3.4 index is used for identifying the El Niño years. SST anomalies of greater than 0.4°C persisting for at least 6 months is the criteria used to identify the El Niño years. The IOD index is defined as the difference in SST anomalies between the western (50°E to 70°E and 10°S to 10°N) and the southeastern (90°E to 110°E and 10°S to 0°) equatorial Indian Ocean (Saji *et al*., 1999). Figure 1 shows the Niño3.4 (solid line) and IOD (dashed line) indices for the 52 years. The positive peaks indicate the positive IOD years.

Sea-surface temperature and wind anomalies

Interannual variability in the Indian Ocean is influenced by ENSO-related warming and Indian Ocean Dipole mode events. It is important to know whether this interannual variability is remotely forced by any external phenomena, such as El Niño, or due to the internal dynamics of the Indian Ocean. To examine such a variability, especially the basin-wide warming in boreal winter and the dipole structure (in boreal autumn) in SST anomalies, the composite maps of SST (Figure 2) and wind anomalies (Figure 3) are prepared and a detailed analysis is made. Figure 2(a–d) shows the composite maps of SST anomalies over the Indian Ocean when there is only El Niño (no IOD) in the Pacific (1951,

DOI: 10.1002/joc

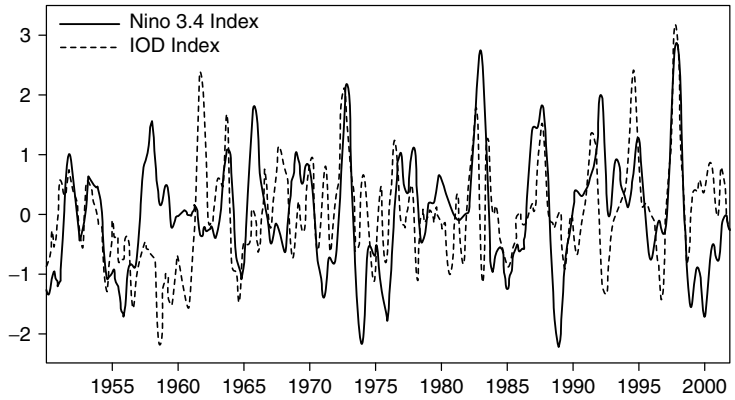

Figure 1. The time series of HadISST anomaly (°C) averaged over the Niño 3.4 region (5 °N to 5 °S and 120 °W to 170 °W) (solid line) and IOD index (dashed line).

1957, 1965, 1969, 1976, 1987 and 1991 (hereafter 'El Niño only') for June to September (JJAS(0)), October to November (ON(0)), December to February (DJF(0/1)) and March to May (MAM(1)), respectively. At the top of each panel, the fraction of area with SST anomalies above 0.1 °C is indicated. This area computation by percentage is to quantify the amount of warming that experiences an SST anomaly higher than 0.1 °C over the Tropical Indian Ocean. During JJAS(0), the positive SST anomalies appear over most of the Arabian Sea, Bay of Bengal and south central Indian Ocean, and about 30% of the area experiences a warming greater than 0.1 °C. By October–November, most of the Indian Ocean region is covered with the positive SST anomalies (53% area >0.1 °C), except in some small pockets in the southeast and western Indian Ocean (Figure 2(b)). This anomalous warming continues into the following winter season as a basin-wide warming over the entire Indian Ocean (76% area >0.1 °C) but weakens by boreal spring (74% area >0.1 °C). During the boreal summer, wind anomalies over the Indian Ocean are very weak (Figure 3(a)). In the boreal autumn, strong easterly wind anomalies are observed over the east equatorial Indian Ocean (Figure 3(b)). However, these easterly wind anomalies weaken by winter (DJF(0/1)) and disappear in the spring season (Figure 3(c) and (d)).

Both El Niño and IOD co-occurred on several occasions (1963, 1972, 1982 and 1997: co-occurrence years). Composite maps of SST and wind anomaly during the co-occurrence years are shown in Figures 2(e–h) and 3(e–h), respectively. About 38% of the area experiences strong warming during JJAS(0), with cooling in the eastern and warming in the western Indian Ocean (Figure 2(e)). During this period, easterly wind anomalies appear (Figure 3(e)) over the eastern equatorial Indian Ocean and are enhanced in the boreal autumn (Figure 3(f)). The strong easterly anomalies cause anomalous upwelling in the Sumatra coast, as pointed out in the earlier studies, which leads to the dipole-like structure in the equatorial Indian Ocean, with strong negative SST anomalies (cooling) in the eastern and positive SST anomalies (warming) in the western equatorial Indian Ocean. Dipole structure in the SST anomalies over the equatorial Indian Ocean peaks during October–November (Figure 2(f)). The eastern cooling is restricted to a smaller region as compared to western warming. The warming is not confined to the south of the equator but extends to its north, including the Bay of Bengal and the Arabian Sea, and the total area covered by the strong warm anomalies encompasses about 70% of the Indian Ocean. By the following winter, the eastern cooling disappears, and the resultant basin-wide warming appears over the Indian Ocean (86% area >0.1 °C) and persists through the boreal spring. The easterly wind anomalies over the east equatorial Indian Ocean migrate to the south of the equator during DJF(1/0) and then disappear by boreal spring (Figure 3(h)).

IOD (positive) occurred on several occasions without El Niño in the Pacific (1961, 1967, 1977 and 1994: hereafter 'IOD only') and the corresponding composites of SST and wind anomalies are shown in Figures 2(i–l) and 3(i–l), respectively. Strong easterly wind anomalies appear in the east equatorial Indian Ocean during the summer monsoon period and these easterly anomalies strengthen by October–November (Figure 3(i) and (j)), similar to that of the co-occurrence composites. There is no easterly component present in the DJF(0/1) and MAM(1) (Figure 3(k) and (l)). Unlike the other two cases, in the IOD-only case, none of the four seasons show any basin-wide warming in the Indian Ocean. The area covered by the strong warm SST anomalies during DJF(0/1) is only about 18% of the Indian Ocean (Figure 2(k)).

It is important to know whether the wintertime basin-wide surface warming signals are present only in the El Niño (or co-occurrence) composites or in any random composites. Initially, we plotted two random composites and compared them with the extreme warming of the co-occurrence events (Figure 4). It is very clear that some of the random composites have a higher degree of warming than the co-occurrence composites (right panel). So it is necessary to know how likely it is that a random composite will experience basin-wide warming (measure of significance) greater than (or equal to) the

DOI: 10.1002/joc

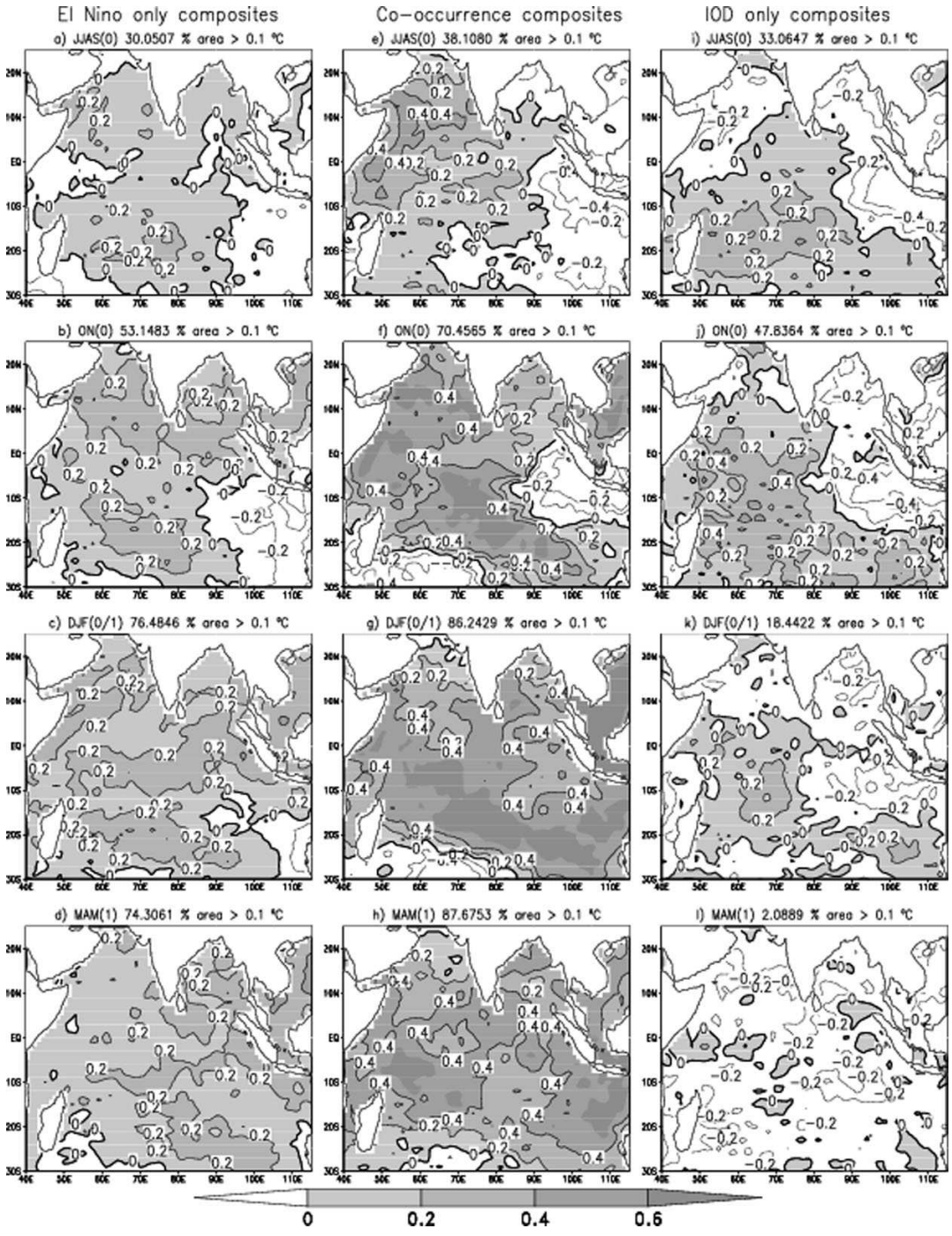

Figure 2. Composite maps of HadISST anomalies for El Niño-only years (a–d), co-occurrence years (e–h) and IOD-only years (i–l) for JJAS(0), ON(0), DJF(0/1) and for MAM(1). Contour interval is 0.2. The fraction of area with SST anomaly above 0.1 °C is indicated at the top of each panel. (1951, 1957, 1965, 1969, 1976, 1987 and 1991 are used for El Niño-only composites, 1963, 1972, 1982 and 1997 for co-occurrence composites and 1961, 1967, 1977 and 1994 for IOD-only composites).

El Niño-only or co-occurrence composites. To test the significance of warming signals during boreal winter in both El Niño-only and co-occurrence composites, we carried out statistical significance tests. Using 4500 random composites, the Probability Density Function (PDF) of the Indian Ocean basin-wide warming area coverage is computed (Figure 5). Figure 5(a) shows that 6% of the random composites experience a warming with amplitude and coverage equal to or greater than the El Niño-only composites. Here, 7 years are used to compute the random composites from all the years. In Figure 5(b), random composites are built using 4 years from all the 52 years and it is found that 4% of the random composites have a warming with amplitude and coverage equal to or

DOI: 10.1002/joc

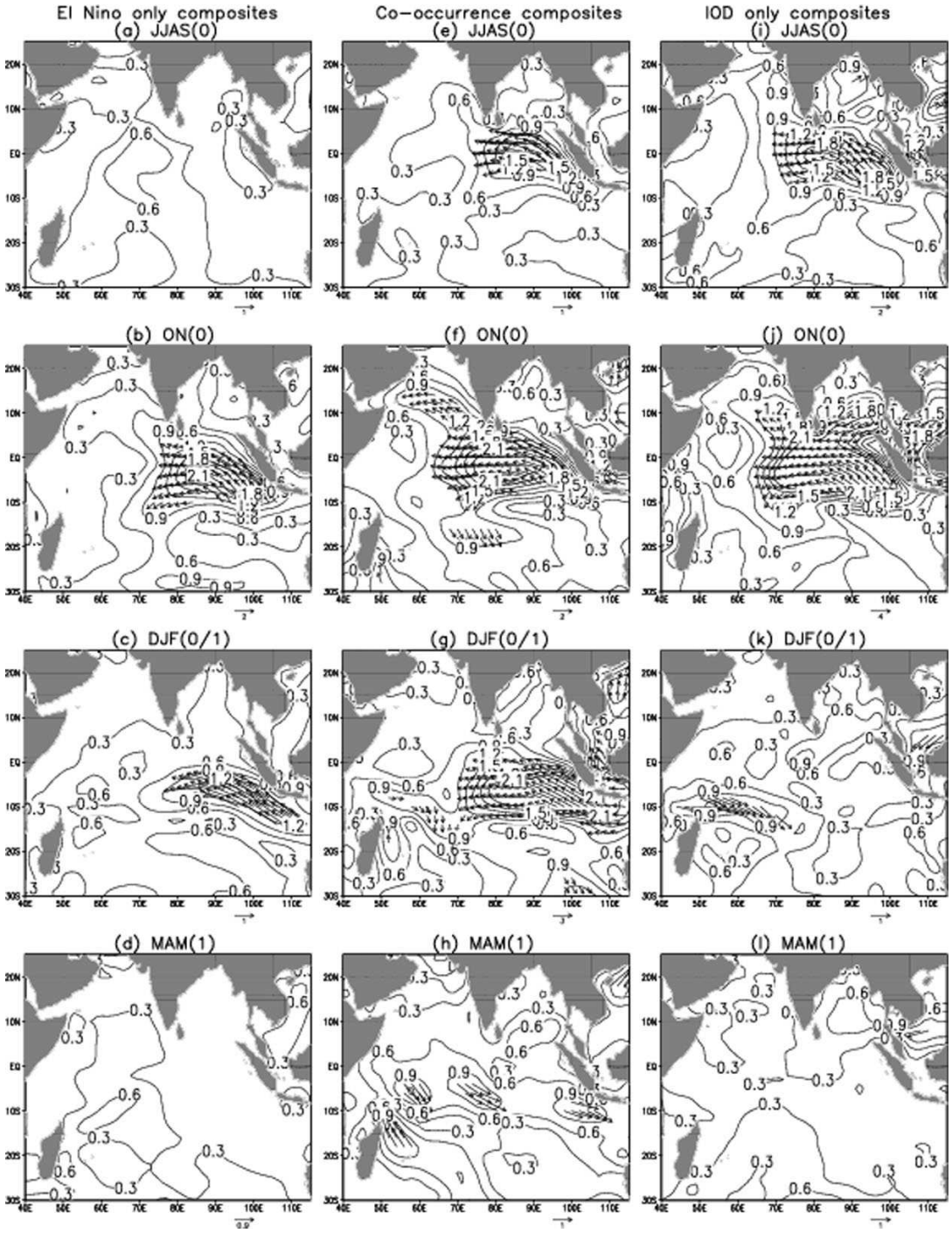

Figure 3. As in Figure 2, but for surface wind speed anomaly (NCEP/NCAR). Contour interval is 0.3 m/s. Vectors indicate the wind direction greater than 0.9 m/s.

greater than the co-occurrence composites. This suggests that the warming patterns are statistically significant at the 94–96% level. Similar analysis is carried out by computing 4500 random composites using 7 years (Figure 5(c)) and 4 years (Figure 5(d)) but excluding all ENSO and IOD years. It is observed that none of the random composites have a higher degree of warming than the El Niño-only or co-occurrence composites. On the basis of the above analysis, it is clear that there are statistically significant basin-wide warming patterns in both El Niño-only and co-occurrence composites during DJF(0/1).

The basin-wide surface (winter) warming occurs during El Niño-only years and co-occurrence years but not in IOD-only years. This shows that the warming is remotely forced by the SST activities of the tropical eastern Pacific.

DOI: 10.1002/joc

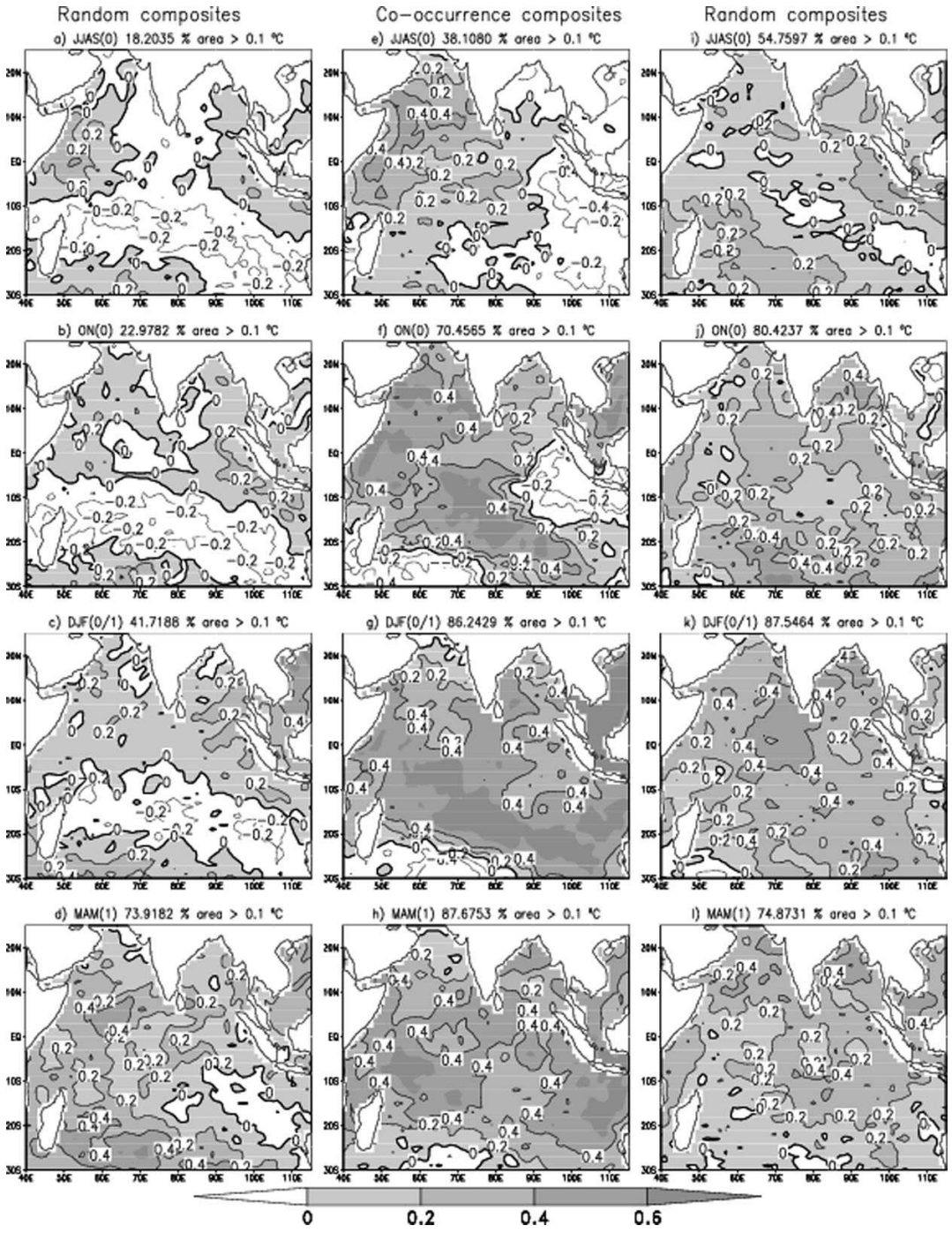

Figure 4. Composite maps of HadISST anomalies for (a–d) Random years (1974, 1968, 1990 and 2000), (e–h) co-occurrence years and (i–l) Random years (1959, 1995, 1979 and 1989), for JJAS(0), ON(0), DJF(0/1) and for MAM (1). Contour interval 0.2. At the top of each panel, the fraction of area with SST anomaly above 0.1 °C is indicated.

However, Klein *et al*. (1999) showed that the magnitude of El Niño influence on the SST anomalies in the remote oceans (Indian Ocean) is typically 0.2 °C to 0.3 °C, with the extreme peak anomalies of 0.5 °C. It is important to note that by October–November the warm anomalies appear in the northern Indian Ocean (north of the equator) in both El Niño-only and co-occurrence composites apart from the southern warming, and basin-wide warming appears in the entire north Indian Ocean by the boreal winter. So the basin-wide warming in the El Niño-only and co-occurrence composites is part of a systematic response with distinct patterns. For the IOD-only composites, warming is restricted only to the western Indian Ocean. The weak SST anomalies are observed (over the western Indian Ocean) in boreal autumn and winter for El Niño-only composites as compared to strong

DOI: 10.1002/joc

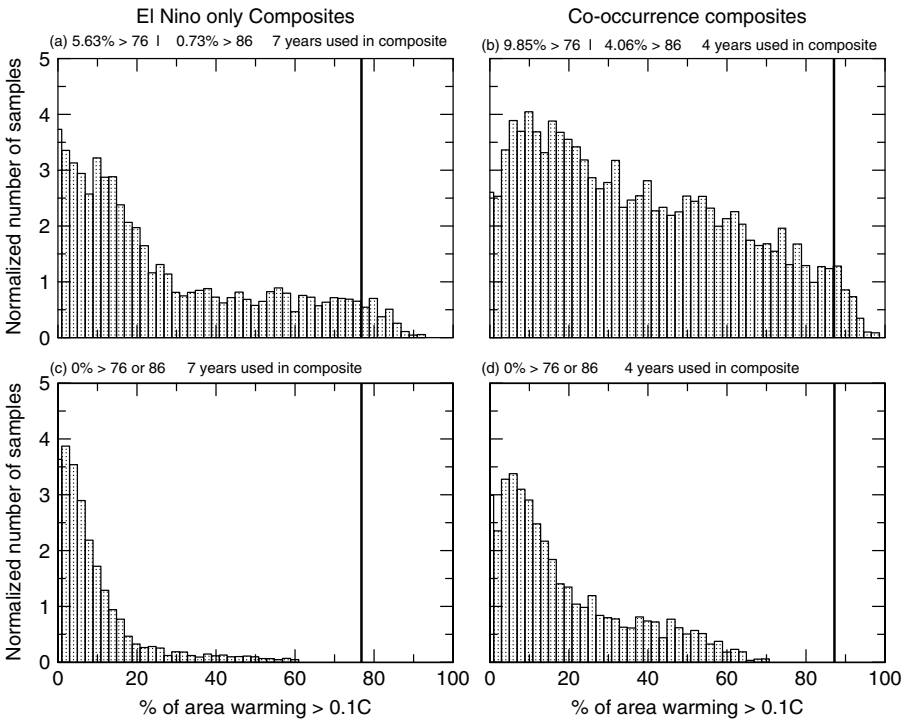

Figure 5. The PDF of random composites (using 4500) of the Indian Ocean basin-wide warming area computed from the HadISST anomalies. (a) and (c) for El Niño-only composites (using 7 years random composites), (b) and (d) for co-occurrence composites (using 4 years random composites). In (a) and (b) the random composites are computed from all the 52 years (1950–2001) and in (c) and (d) the random composites are computed from 37 years (which excludes the IOD, El Niño and co-occurrence years).

anomalies in the co-occurrence composites. In the co-occurrence years, the ENSO influence over the Indian Ocean is modulated by IOD (Bracco *et al*., 2005). This clearly brings out the fact that the western equatorial Indian Ocean warming is mainly contributed by Indian Ocean internal dynamics (IOD related) rather than any remote forcing. It is important to note here that the ENSO, on average, is related to SST anomalies in the remote oceans but is not the sole determining factor for the SST changes in the far away sites (Lanzante, 1996). During the peak phase of IOD, strong easterly wind anomalies appear in the southeastern equatorial Indian Ocean. These winds directly influence the surface circulation, especially along the equator (this is discussed in detail in the next section). By the following winter season, easterly wind anomalies disappear in the IOD-only composites and weaken in the El Niño-only composites. However, these anomalous easterlies in the southeastern Indian Ocean persist in the following winter in the case of the co-occurrence composites.

Surface circulation

The dynamical response of the upper ocean is very similar to the seasonal surface wind forcing, mainly in the north Indian Ocean. The flow of surface currents in the southwest monsoon season is quite the reverse of that in the northeast monsoon season, especially in the Arabian Sea and Bay of Bengal. During the monsoon transition periods, strong eastward jets (currents), called *Wyrtki Jets* (Wyrtki, 1973), appear along the equator on the surface. The composite maps of total surface currents over the Indian Ocean for El Niño-only years in the boreal autumn are shown in Figure 6(a), which is similar to that of the climatological circulation (figure not shown). The strong eastward jets along the equator with the zonal velocity component (contours) exceeding 60 cm/s are clearly seen. Presence of weak easterly wind anomalies (Figure 3(b)) in the east equatorial Indian Ocean does not affect the surface circulation along the equator. In the case of the IOD-only and co-occurrence composites, eastward jets are weakened (Figure 6(b–c)). This shows that most of the variability related to surface circulation is due to the local IOD forcing rather than El Niño forcing. It is worth mentioning here that during the strong positive IOD years (IOD index defined by Saji *et al*. (1999) greater than 2.0) the equatorial jets reverse its direction. Hence, El Niño-related changes in the circulation pattern are not significant during these years.

Subsurface temperatures and isopycnal depths

It is understood that basin-wide surface warming of the Indian Ocean in different seasons (mainly in boreal autumn and the following winter) is remotely forced by El Niño-related signals from the eastern Pacific. Previous studies (Rao *et al*., 2002; Feng and Meyers, 2003; and so on) have suggested that significant temperature anomalies would develop in the subsurface early in the summer monsoon months and reach their peak during

DOI: 10.1002/joc

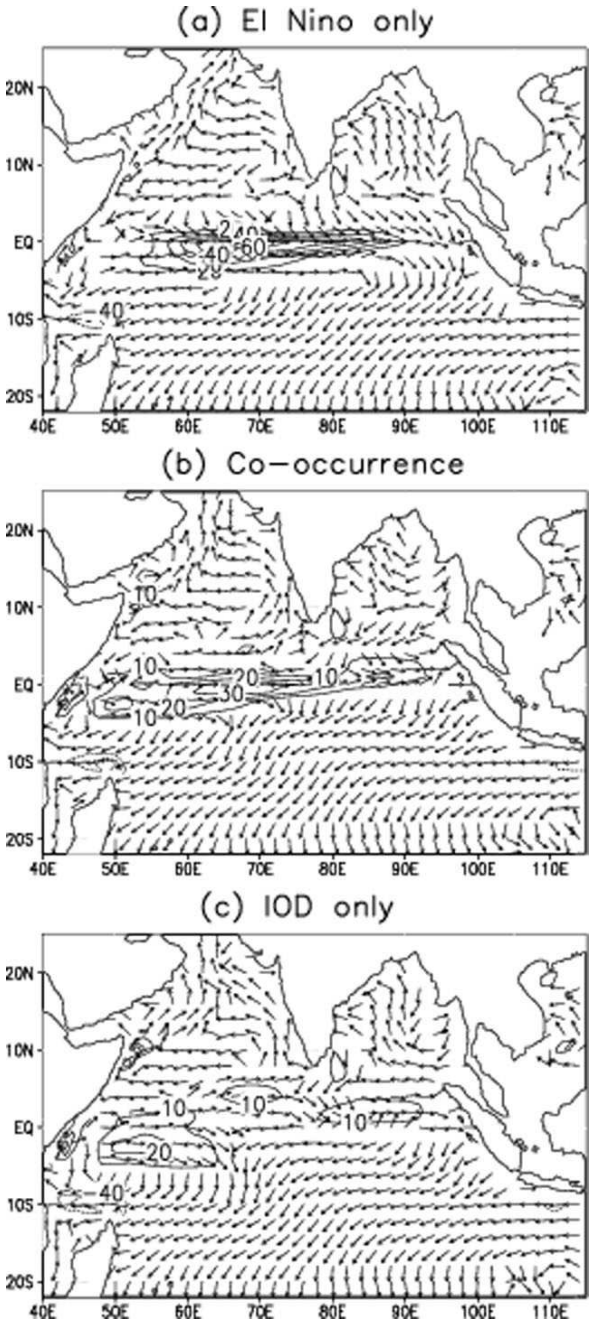

Figure 6. Composite maps of SODA surface currents (vectors) and the zonal component of currents (contours cm/s) during the post-monsoon period (ON) (contour interval 10 cm/s), (a) for El Niño-only years, (b) for co-occurrence years and (c) for IOD-only years.

October–November. So in this context it is important to know whether the wintertime basin-wide warming persists in the subsurface temperature anomalies. SODA temperature profiles are used to understand the subsurface variability. Shenoi *et al*. (2005) showed that the difference in climatological seasonal cycle of temperature (upper 50 m) between SODA and Levitus (Levitus and Boyer, 1994) is within 0.5 °C for the north Indian Ocean.

Figure 7 shows the composite maps of temperature anomalies at the isopycnal $\sigma_o = 25.0$ for El Niño-only (a–d), co-occurrence (e–h) and IOD-only (i–l) years for all the four seasons. The spatial distributions of the temperature anomalies at the isopycnal $\sigma_o = 25.0$ are similar to that at 100 m depth (not shown). So the analysis of temperature anomalies at the isopycnal ($\sigma_o = 25.0$) reflects the subsurface variability as well as changes in the temperature at constant density level. However, the magnitudes of temperature anomalies are less in the case of the isopycnal ($\sigma_o = 25.0$) than that at 100 m depth. The isopycnal ($\sigma_o = 25.0$) layer encloses the whole upper Indian Ocean north of 25 °S in the annual mean picture (figure not shown). The depth of the isopycnal ($\sigma_o = 25.0$) layer is about 120 m in the eastern Indian Ocean (north of 15 °S) and it shoals up to about 80 m near 7 °S, 60 °E, this is similar to the findings of Zhang and Talley (1998). The annual mean isopycnal depths for the Indian Ocean vary within the range of the winter mixed layer (Rao *et al*., 1989). The reason for selecting the isopycnal layer of $\sigma_o = 25.0$ is that the layers less than $\sigma_o = 25.0$ (depth) do not cover the entire Indian Ocean. In the El Niño-only composites, none of the four seasons experience basin-wide subsurface warming in the Indian Ocean. In boreal autumn, strong positive anomalies are present in the eastern (south of the equator) Indian Ocean (Figure 7(b)). In the case of co-occurrence composites, strong positive anomalies appear in the western Indian Ocean and negative anomalies in the eastern equatorial Indian Ocean (Figure 7 (f)). A similar structure is seen in the subsurface for the IOD-only composites (Figure 7(j)). Moreover, there is no basin-wide warming observed in the subsurface or surface level in the IOD-only composites. During both co-occurrence composites and IOD-only composites, the Arabian Sea shows anomalous warming from boreal autumn to the following spring.

Figure 8 shows the isopycnal ($\sigma_o = 25.0$) layer depth anomaly for the boreal autumn and winter seasons for the three composites. In the El Niño-only composites (Figure 8(a) and (b)), weak (positive or negative) isopycnal depth anomalies are noticed in both the seasons over most of the Indian Ocean, except in the south central region. In the case of the co-occurrence and IOD-only composites, isopycnal depths deepen over the western Indian Ocean (positive anomaly) and shoal over the eastern Indian Ocean for the two seasons. The shoaling of isopycnal depth is due to upwelled subsurface water and the deepening is due to downwelling. Deepening or shoaling of isopycnal depths is stronger in IOD-only composites as compared to the other two composites.

Sea-Surface Height (SSH) and heat content anomalies

In this section, SODA SSH anomaly is used to examine the role of ocean dynamics on western Indian Ocean warming for the three cases (El Niño-only, IOD-only and co-occurrence composites). The Root Mean Square RMS difference between TOPEX/POSEIDON (satellite data)

DOI: 10.1002/joc

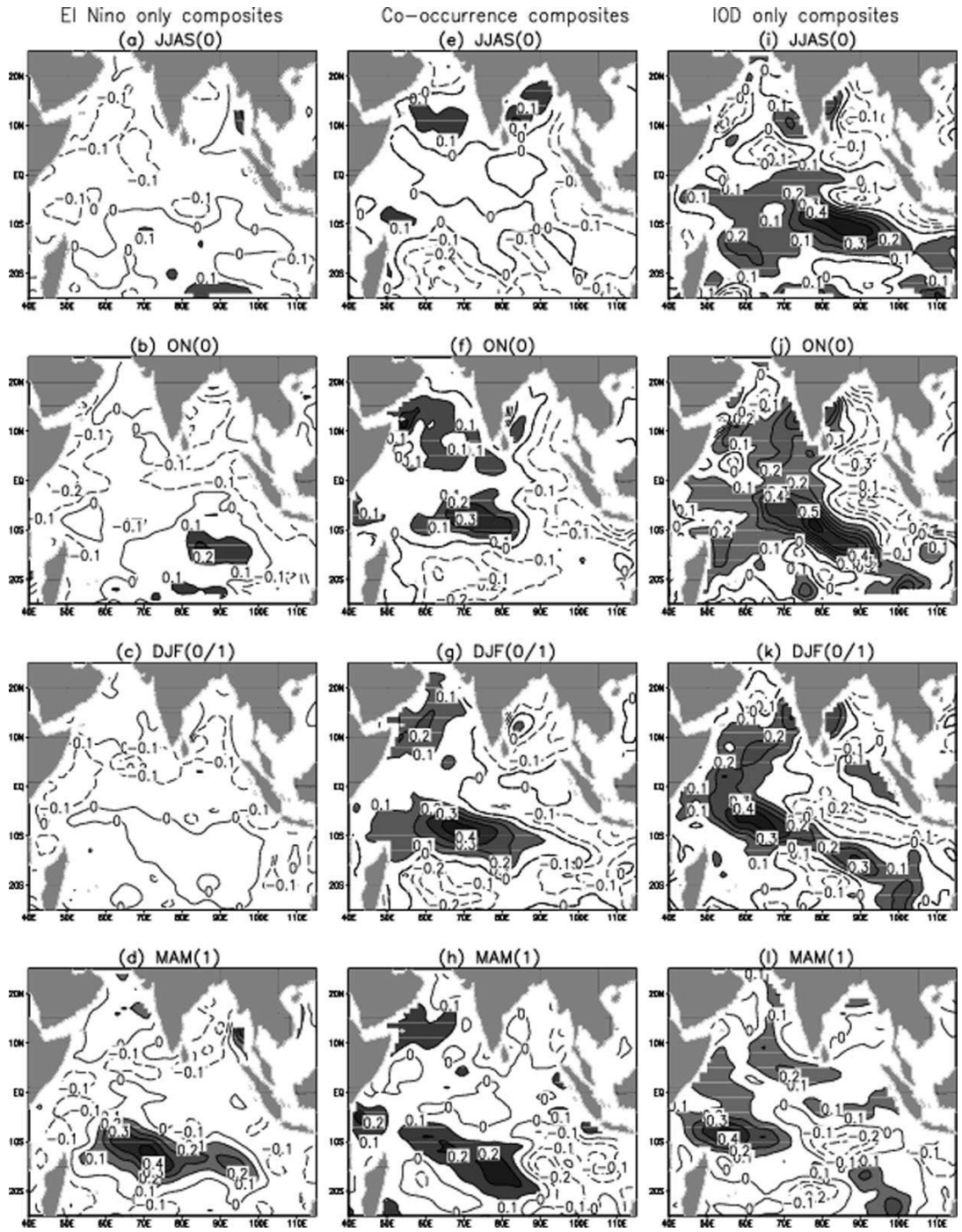

Figure 7. As in Figure 2, but for the SODA temperature anomalies at isopycnal ($\sigma_o = 25.0$) layer. Contour interval is 0.1 °C.

and SODA SSH anomalies for the 9-year (1993–2001) annual climatology is less than 1.2 cm. The spatial map shows an RMS difference of about 5 cm over the Somali coast and less than 3 cm over most of the Indian Ocean. Figure 9 displays the time-longitude plots of SSH anomaly composites along 10 °S over the Indian Ocean. In the case of El Niño-only composites, the positive SSH anomalies found in the central Indian Ocean during the boreal autumn show very weak westward propagation (Figure 9(a)), while in the other two cases, strong westward propagating SSH anomalies are observed, which reach the western boundary by the following boreal winter (Figure 9(b) and (c)). The analysis of spatial and temporal distribution of heat content (upper 250 m) anomalies for the El Niño-only composites reveals that the positive heat content anomalies appear in the eastern Indian Ocean (east of 70 °E), including the Bay of Bengal, during boreal summer (figure not shown), which is similar to

DOI: 10.1002/joc

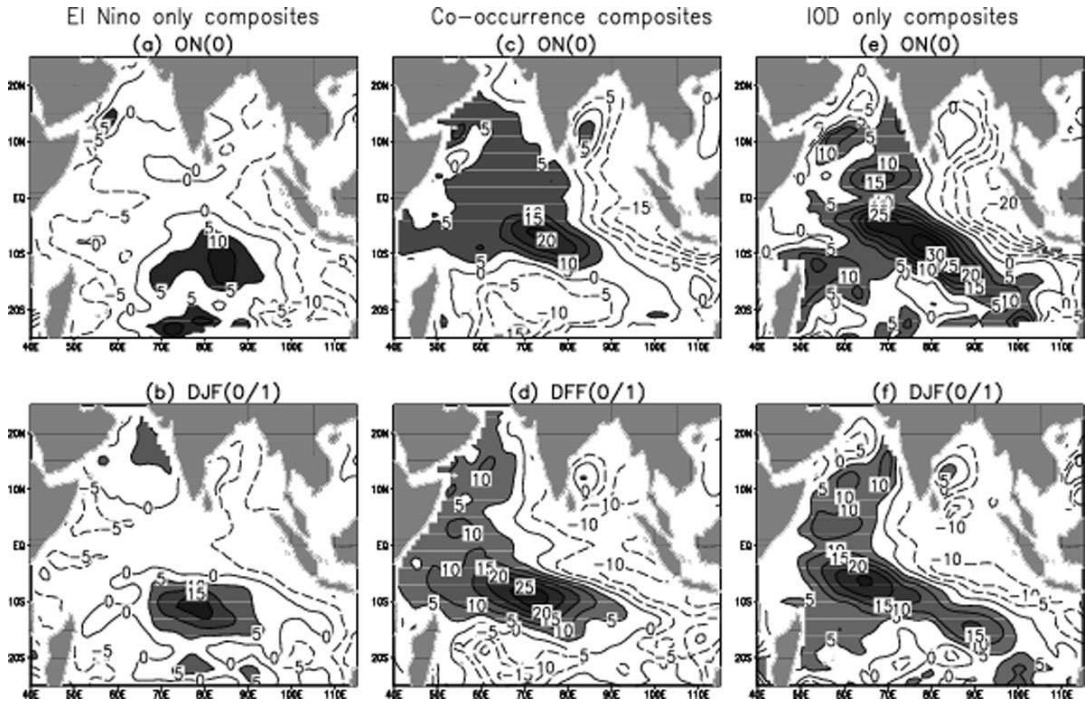

Figure 8. Composite maps of isopycnal layer depth anomalies for boreal autumn and winter: (a), (b) for El Niño-only composites; (c), (d) for co-occurrence composites; and (e), (f) for IOD-only composites, from SODA temperature and salinity data. Contour interval is 5 m.

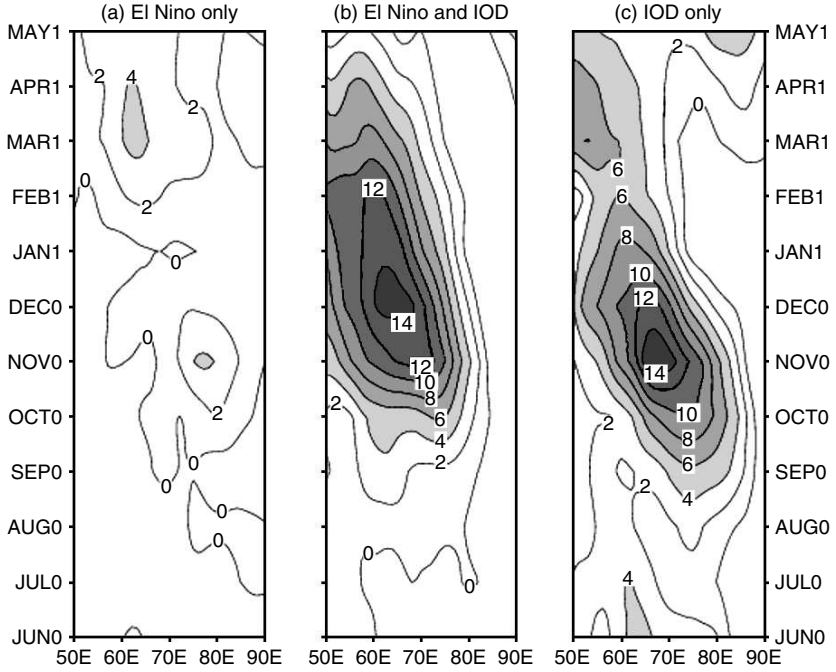

Figure 9. Time–longitude plots of SODA sea-surface height anomaly (cm): (a) El Niño-only composites, (b) co-occurrence composites and (c) IOD-only composites. Contour interval is 2 cm and the interval above 4 cm is shaded.

the spatial distribution of SSH anomalies. The magnitudes of the positive heat content anomalies increase in the central Indian Ocean but decrease towards the east by October–November. The maximum heat content anomalies (positive) are observed in the region south of the equator, which extend westward in the following winter and spring seasons. The heat content anomalies observed in the winter and spring (positive in the east and negative in the west) have a structure similar to the subsurface temperature anomalies. Like the surface dipole in

DOI: 10.1002/joc

the SST anomaly, heat content anomalies also showed a dipole-like structure, with negative anomalies in the eastern equatorial Indian Ocean and positive anomalies in the western equatorial Indian Ocean for co-occurrence and IOD-only composites, respectively (Figure not shown). A strong gradient is observed only in the region south of the equator. Initially, during the summer months, the existence of strong positive anomalies near 85 °E 10 °S is observed. These maximum positive anomalies gradually propagate westward and reach the western boundary by the following boreal winter.

The westward propagation seen in the heat content anomalies (or SSH anomaly) is associated with the off-equatorial Rossby waves, which further confirms the role of ocean dynamics in warming the western Indian Ocean for the next season. Absence of such a strong propagation in El Niño-only composites (either in heat content or in SSH anomalies) suggests that the El Niño alone does not induce an Indian Ocean dynamical signature (e.g tropical Rossby waves) unless the IOD coupled mode is also excited. The El Niño-related signals on the dynamic response of the Indian Ocean are weaker than the local phenomena. It is also important to note that there is no basin-wide subsurface warming in any of the three cases, as seen in the surface. The strong propagation of SSH anomalies in IOD-only and co-occurrence composites and absence of such a propagation in El Niño-only composites indicate that basin-wide (especially western Indian Ocean) surface warming in El Niño-only composites is not exactly governed by the planetary wave propagation. To further strengthen this hypothesis, it is necessary to examine the air–sea fluxes and their contribution to surface warming or cooling, which is discussed in the next section.

Surface fluxes

Latent heat flux anomalies for El Niño-only composites for the four seasons are shown in Figure 10(a–d). During boreal autumn (Figure 10(b)), most of the region except the southeast Indian Ocean (south of 5 °S) has negative latent heat flux anomalies (dashed line). This shows that the ocean in this region loses relatively less heat to the atmosphere in the El Niño-only years. The negative anomalies continued to persist in the following winter (Figure 10(c)) over almost the entire Indian Ocean and the positive anomalies weaken in the southeastern parts. At the same time, basin-wide warming is observed in the winter season (Figure 2(c)). So the latent heat flux contributed considerably to the warming in the El Niño-only composites. Figure 10(e–h) displays the composite anomalies of latent heat fluxes for the co-occurrence years. During the summer monsoon (Figure 10(e)), both western and eastern parts of the Indian Ocean have positive anomalies. The core of positive anomalies during October–November (Figure 10(f)) is seen in the south-central to eastern Indian Ocean (between the equator and 10 °S). At the same time, the western Indian Ocean, especially south of the equator, maintained strong negative latent heat flux anomalies, which resulted in positive SST anomalies over that region. In the following winter (Figure 10(g)), the basin-wide negative latent heat flux anomalies look different from the El Niño-only composites, but there is basin-wide warming in the Indian Ocean (Figure 2(g)). The western warming in the boreal autumn during the co-occurrence composites is stronger than the El Niño-only composites. This warming continues into the next season, and the ocean dynamics play an important role in maintaining the winter (following winter) warming. The weak positive latent heat flux anomalies are not sufficient to reduce the SST anomalies in the western Indian Ocean. Klein *et al*. (1999) also reveal that the positive SST anomalies in the southwestern Indian Ocean are the direct response of ocean dynamics instead of surface heat fluxes. Hence, strong basin-wide warming persisted in the following winter for the co-occurrence composites. For the IOD-only composites, a similar type of patterns in the latent heat flux anomalies appears in the following winter, but no basin-wide warming is observed over the Indian Ocean, unlike for the co-occurrence composites. In fact, this is due to the absence of El Niño-related (ENSO) subsidence over the eastern Indian Ocean in the following winter. On the other hand, in the co-occurrence composites, the positive short wave flux (incoming solar radiation) anomalies (Figure 11(g)) due to the clear sky radiation are favorable for the warming, and this further supports the findings of Klein *et al*. (1999). However, for IOD-only composites, no such warming is observed over the eastern Indian Ocean owing to the absence of strong positive short wave flux anomalies in the boreal winter (Figure 11(k)). From the above discussion it is clear that in El Niño-only composites, surface heat fluxes (mainly latent heat flux and short wave radiation) play a major role in maintaining the basin-wide surface warming in the Indian Ocean, whereas, in the co-occurrence years, the ocean dynamics is responsible for warming in the western Indian Ocean, and the latent heat flux and solar radiation cause the warming in the eastern Indian Ocean.

Heat budget

We have carried out upper ocean heat budget analysis to diagnose the role of surface fluxes and ocean dynamics in maintaining the wintertime basin-wide warming during the El Niño-only years and co-occurrence years. In the present study, SODA temperature, zonal, meridional and vertical currents and COADS heat fluxes are used to estimate the heat budget of the upper 50 m in the southeastern (90 °E–110 °E and 10 °S to the equator) and western (50 °E–70 °E and 10 °S–10 °N) tropical Indian Ocean. Recently, Shenoi *et al*. (2005) computed the heat budget for the northern Indian Ocean (Arabian Sea and Bay of Bengal) using SODA products. They found that the SODA heat budget (for 30 years' climatology, from 1963–1992) is well comparable with the heat budget computed using a variety of other data sets of Shenoi *et al*. (2002). We also did similar experiments over the equatorial Indian Ocean using 30 years' climatology and

DOI: 10.1002/joc

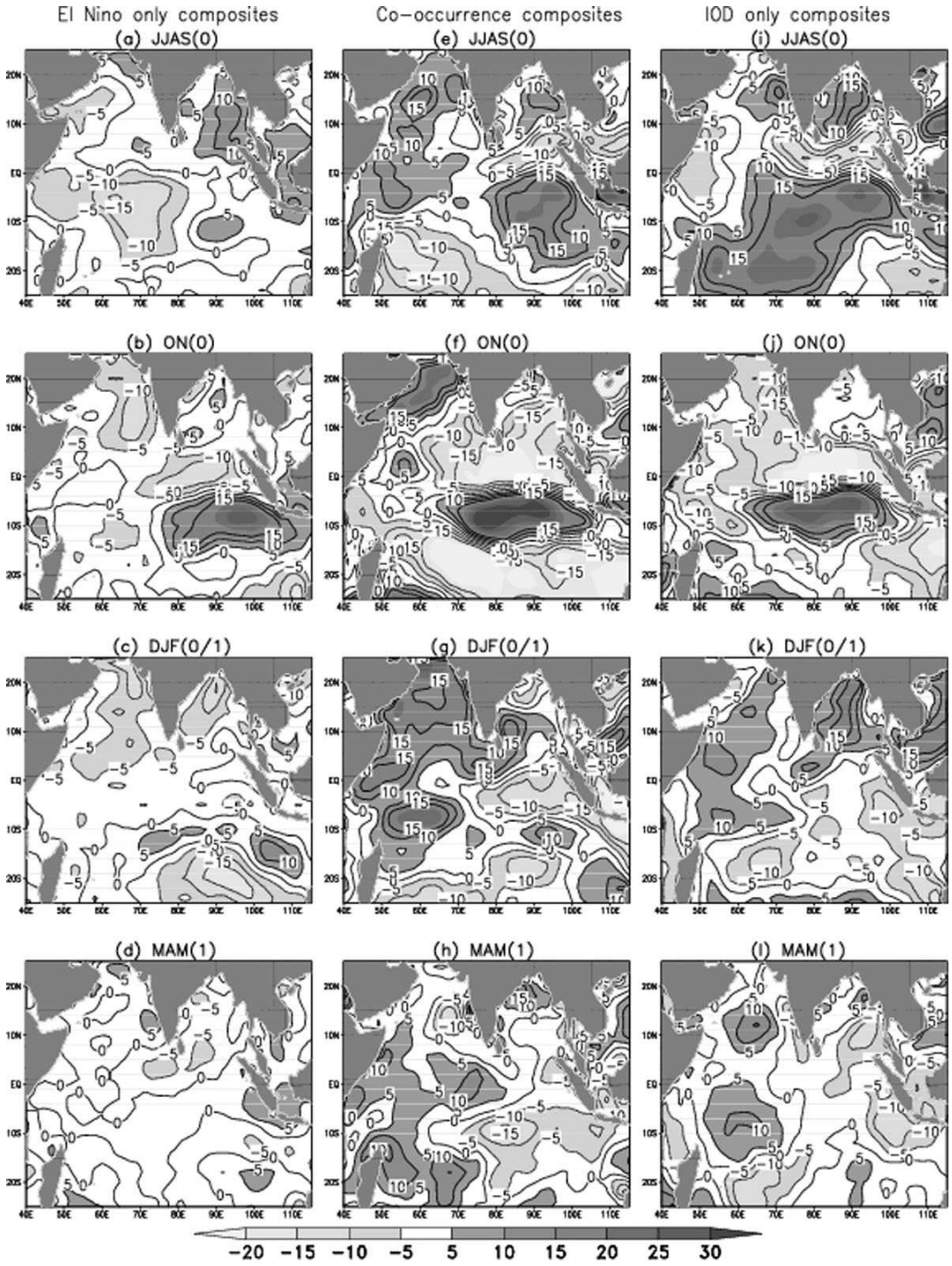

Figure 10. As in Figure 2, but for NCEP/NCAR latent heat flux anomaly. Contour interval is 5 W/m^2.

found that the heat budget balances in the region (within the standard deviation) during the fall, winter and spring seasons (figure not shown). Figure 12 shows the balance of heat budget in the control volume over the southeastern Indian Ocean and western Indian Ocean for all the three composites (El Niño-only, co-occurrence and IOD-only years). The thin and continuous line shows the heat content tendency, the dashed line represents the sum of the other terms (Qt, horizontal and vertical advection, heat flux and diffusion) and the thick continuous lines show the standard deviation of the heat content tendency. In the southeastern Indian Ocean, both heat content tendency and Qt are in phase with each other most of the time. Qt is mostly within the standard deviation of heat content tendency for all the three composites. Qt is always within the standard deviation in the western

DOI: 10.1002/joc

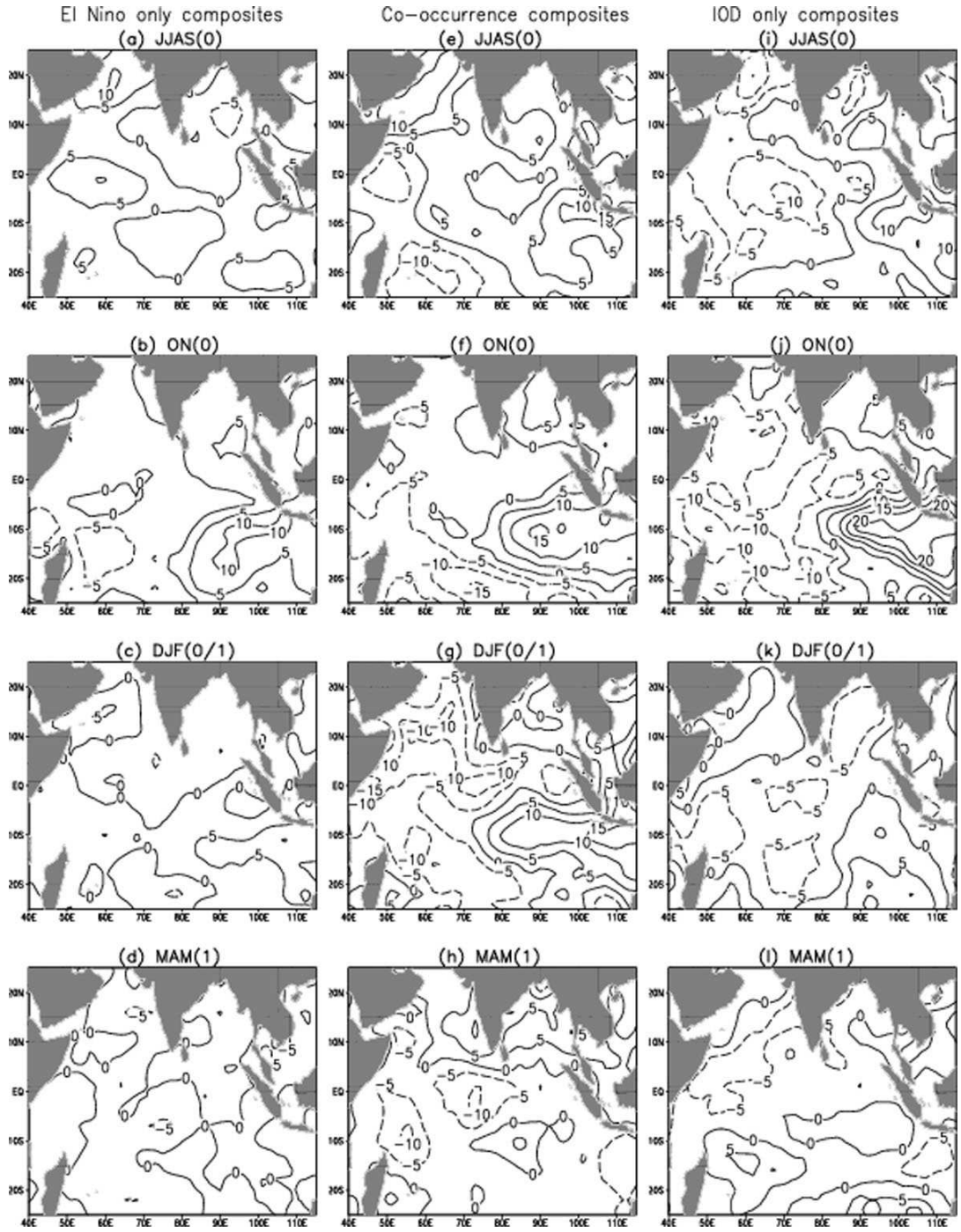

Figure 11. As in Figure 2, but for NCEP/NCAR short wave radiation anomaly. Contour interval is 5 W/m^2.

Indian Ocean, except in June(0), July(0), April(1) and May(1), and the pattern is similar to that of heat content tendency. The uncertainties or errors associated with the heat budget come from the estimates of the heat content, surface heat fluxes and vertical advection. Wyrtki and Ulrich (1982) found that the errors are about 15% of the mean annual cycle for the estimates of heat content in the upper 100 m of the north Pacific. Weare and Strub (1981) found the random errors on net heat fluxes due to sampling biases on monthly means to be about 10% of the mean. However, for heat budget calculations, it is assumed that most of the random errors would get cancelled over averaging and finally only the systematic error will dominate (Hareesh Kumar and Mathew, 1997).

Figure 13 shows the composites of (a) Heat Content Anomaly (HCA) tendency term, (b) meridional advection anomaly, (c) zonal advection anomaly, (d) vertical

DOI: 10.1002/joc

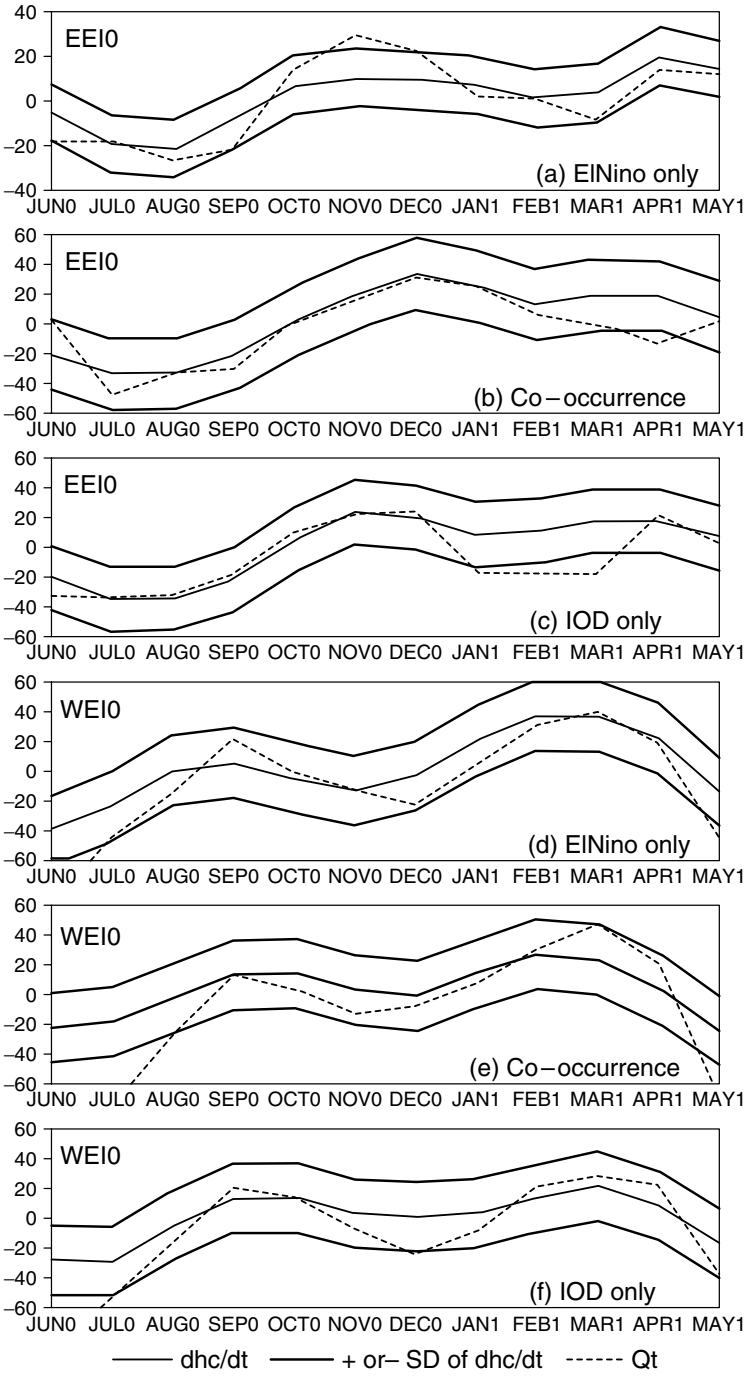

Figure 12. Heat budget balance (a) to (c) for the southeastern equatorial Indian Ocean and (d) to (e) for the western equatorial Indian Ocean for all three composites. Units are in W/m^2.

advection anomaly, (e) net heat flux anomaly and (f) diffusion anomaly over the southeastern Indian Ocean. In the El Niño-only composites, HCA tendency shows a slight decrease in JJAS(0) (compared to the previous season) and an increase in DJF(0/1) over the southeastern Indian Ocean (Figure 13(a)). As compared to the other two composites, the rate of change (or tendency) of HCA is very low in the El Niño-only composites. During the El Niño-only years, both the horizontal (meridional and zonal) and vertical advection anomalies are close to zero in all the four seasons. This shows that the contribution of horizontal and vertical advection for change in HCA is less (Figure 13(b–d)). However, variations in the heat flux anomalies are consistent with the HCA tendency. A decreasing trend in the HCA tendency is observed from June to August, and at the same time negative heat flux anomalies are present up to September over this region (Figure 13(e)). The HCA tendency shows a positive

DOI: 10.1002/joc

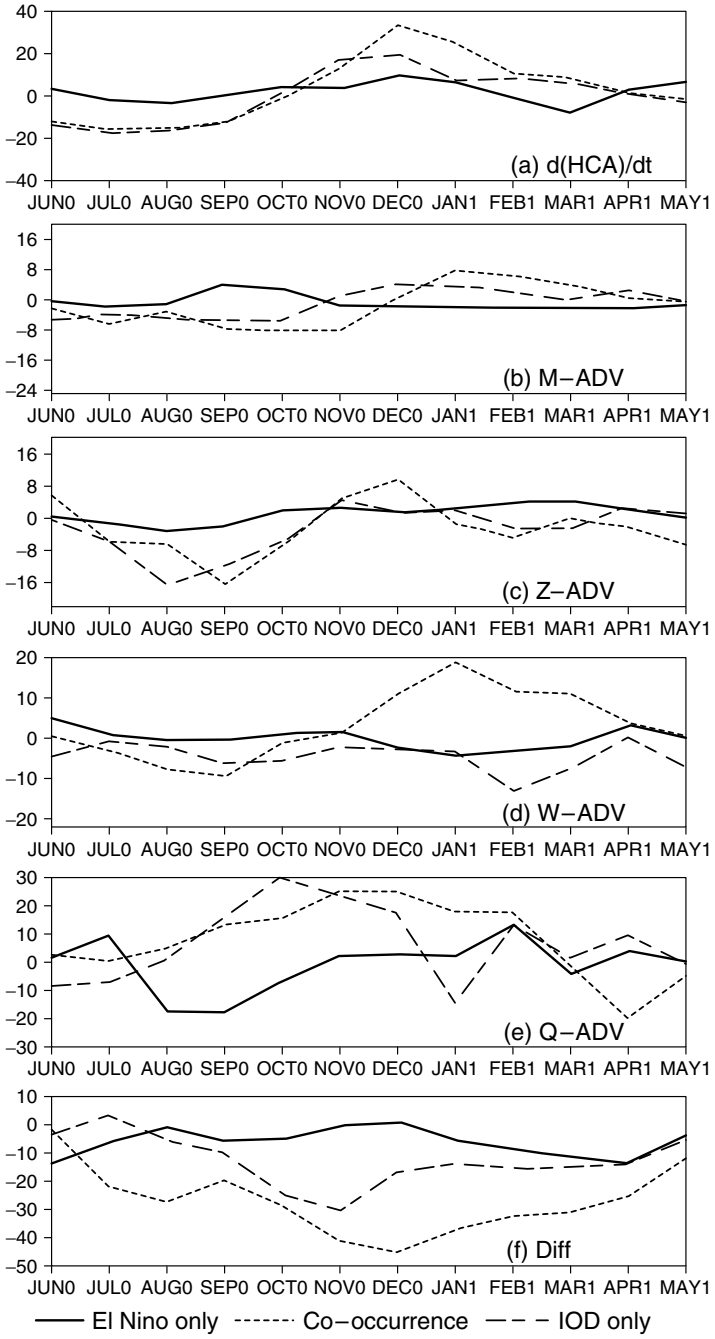

Figure 13. Heat budget analysis (50 m). (a) Heat content anomaly tendency, (b) meriodional advection anomaly, (c) zonal advection anomaly, (d) vertical advection anomaly, (e) heat flux anomaly and (f) diffusion anomaly for all three composites over the southeastern equatorial Indian Ocean. Units are in W/m^2.

trend up to December, when the heat flux anomalies start increasing from its minimum. This further supports (see Section on Surface Fluxes) the fact that the heat fluxes are mainly responsible for SST anomaly variations in the El Niño-only composites. We also computed the HadISST anomaly tendency for the El Niño-only composites over the eastern Indian Ocean, which showed significant variations from the boreal autumn to winter (DJF(0/1)) season. This is because heat flux normally has more influence on the surface temperature than the subsurface temperature. Loss of heat from the control volume due to diffusion is almost close to zero during most of the time (Figure 13(f)).

In the co-occurrence composites, HCA tendency shows negative sign during the boreal summer, and from autumn onwards it changes to positive. The increasing tendency in HCA is more in the co-occurrence composites than the IOD-only composites during DJF(0/1) (with

DOI: 10.1002/joc

reference to JJAS). This indicates the existence of strong positive SST anomalies in the boreal winter over the southeastern Indian Ocean during the co-occurrence years. The contributions of zonal and vertical advections (Figure 13(c–d)) are more in the boreal summer and autumn seasons, resulting in large cooling over the eastern Indian Ocean (Figure 13(a)). The contribution of horizontal advection in controlling the HCA changes decreases towards the end of November and remains weak in the next two seasons. Even though meridional advection anomaly shows some variations, which is always weaker than zonal advection, there are notable differences between meridional and zonal advection anomalies during the winter season in the co-occurrence composites (Figure (13(b) and (c)). Weak positive meridional advection anomalies are noticed in DJF (0/1), while zonal advection showed negative anomalies. This shows that there is very little contribution of meridional advection to warming the southeastern Indian Ocean in DJF (0/1), and the contribution is much weaker than vertical advection and heat flux. During the strong positive IOD years (independent of El Niño), upwelling starts from early June and strengthens by October–November. The strong upwelling induced cold water is advected northwestward along the coast of Sumatra and westward along the equator. Vertical advection over the southeastern Indian Ocean does not show strong upwelling during the boreal summer and autumn in the co-occurrence and IOD composites (Figure 13(d)). This is due to the fact that the composites contain both weak and strong IOD events. During the weak positive IOD events, the role of vertical advection is very reduced compared to horizontal advection. In the co-occurrence composites, upwelling is replaced by downwelling from winter onwards (Figure 13(d)), which warms the surface with primary contribution from the surface heat flux. Strong positive heat flux anomalies are observed in boreal autumn and winter, which peak in December and January (Figure 13(e)); this mainly influences the wintertime warming during the co-occurrence years over the southeastern Indian Ocean. Towards the end of November, positive net heat flux is observed owing to cold SST anomalies and weak winds, resulting in the reduction of latent heat loss. The heat loss due to diffusion was maximum in December. From January, there was decrease in the heat loss over the southeastern Indian Ocean due to diffusion (Figure 13(f)). During the IOD-only composites, the changes associated with the upper ocean temperature (or heat content) anomalies are similar to those of co-occurrence years. However, the main difference occurred during DJF (0/1), where the magnitude differs in HCA tendency. The role of horizontal (both meridional and zonal) advection is almost the same in both co-occurrence and IOD-only composites. Also, weak upwelling is observed during DJF (0/1) in the IOD-only composites whereas downwelling is observed in the co-occurrence composites. Nevertheless, there exists some positive heat flux anomaly during boreal autumn, which is not seen to persist during the DJF (0/1) season. Therefore, the absence of positive heat flux anomalies and the presence of weak upwelling have contributed to the increase in HCA tendency over the eastern Indian Ocean during the winter season. Diffusion anomaly during the IOD-only composites showed that heat loss over this region due to this process is maximum during the peak phase of IOD (ON (0)), while in the other seasons the heat loss due to diffusion is reduced.

Over the western Indian Ocean, HCA tendency (Figure 14(a)) showed a decreasing trend during boreal autumn in El Niño years and an increasing trend from December onwards. This is consistent with the SST anomaly composite maps in Figure 2. During IOD-only composites, an exactly opposite trend (compared to El Niño-only composites) in HCA tendency is observed, with increasing trend during ON(0) and decreasing trend in DJF(0/1). The increasing trend of HCA in western Indian Ocean during ON(0) for IOD-only composites is a characteristic feature associated with the IOD formation, which is due to the anomalous meridional advection, and the downwelling along with some contribution from net heat flux during boreal fall. The role of zonal advection in warming the western Indian Ocean is very limited. The weak negative SST anomaly or HCA tendency in the western Indian Ocean during DJF(0/1) is due to meridional advection, reduced upwelling and heat flux anomalies, whereas in the El Niño-only composites the warming in the western Indian Ocean is mainly due to the influence of surface heat flux, with some contribution of vertical advection. Figure 14(e) shows that the surface net heat flux anomaly (solid line) is always positive from boreal summer to winter in the El Niño-only composites. In the case of co-occurrence composites, the initial warming in ON(0) is related to the IOD phenomenon, and warming in the DJF(0/1) is a combined effect of both meridional advection and heat flux. Figure 14(b) shows positive meridional advection anomalies during the DJF(0/1) season, which are responsible for the increase in HCA tendency. Though net heat flux also showed (Figure 14(e)) an increasing trend from November to February (following year), heat loss from the control volume due to diffusion is very little in all the three cases (Figure 14(f)).

CONCLUSIONS

Surface wind anomalies during the El Niño-only composites show the existence of easterly wind anomalies over the southeastern Indian Ocean in boreal summer and autumn. These easterly wind anomalies are weak in magnitude as compared to the co-occurrence or IOD-only composites. The weak easterly wind anomalies in the El Niño-only composites do not weaken the Wyrtki Jets, whereas surface Wyrtki Jets are reversed during October–November in the strong IOD years.

The basin-wide warming in the Indian Ocean occurred in the El Niño-only and the co-occurrence years. In the

DOI: 10.1002/joc

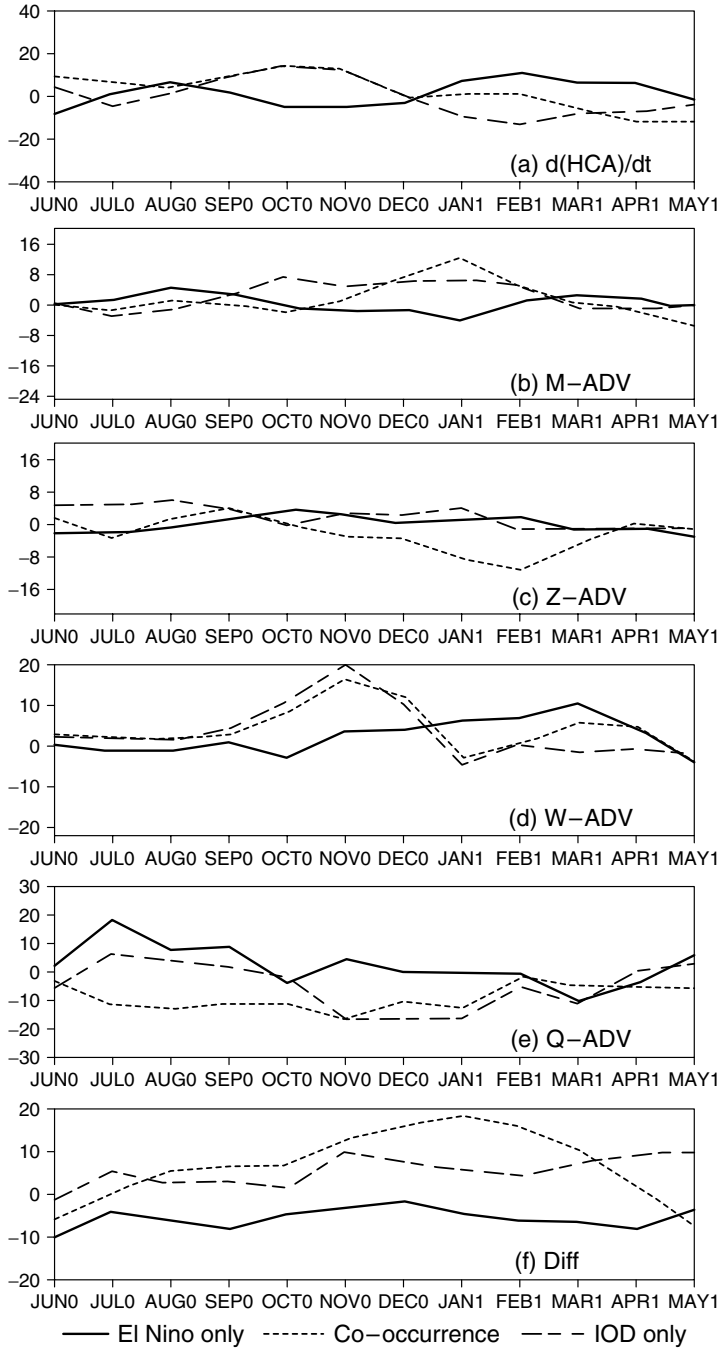

Figure 14. Same as Figure 13, but for the western equatorial Indian Ocean.

case of subsurface warming, an opposite structure in heat content anomaly was noticed during winter between the eastern and western Indian Ocean. During El Niño-only years, heat content anomaly is negative in the western and positive in the eastern Indian Ocean, while it is the opposite in the IOD-only and co-occurrence years. Strong westward propagation of heat content (or SSH) anomalies in the southern Indian Ocean is observed for positive IOD composites. This propagation is associated with the off-equatorial Rossby waves. Such strong propagation is not seen in the case of El Niño-only composites, which suggests that the ocean dynamics play an important role in warming the western Indian Ocean for the IOD composites.

The examination of surface heat fluxes for the three cases revealed that, for the El Niño-only composites, surface heat fluxes (mainly latent heat flux and short wave radiation) play an important role in maintaining the basin-wide wintertime surface warming in the Indian Ocean. Whereas in the co-occurrence years, western Indian Ocean warming is mainly due to ocean dynamics and the eastern warming is due to latent heat flux and

DOI: 10.1002/joc

solar radiation. The suppressed coastal upwelling over Sumatra is also favorable for the eastern warming. No such warming is observed in the IOD-only years. This is due to the absence of El Niño-related (ENSO) subsidence and the resultant reduction in solar radiation over the eastern Indian Ocean in the following winter. The heat budget analysis reveals that the influence of surface fluxes on basin-wide winter warming (cooling) over the western (eastern) Indian Ocean is significant during the El Niño-only years while the heat budget analysis over the southeastern Indian Ocean shows that the downwelling and surface heat flux play an important role in winter warming during the co-occurrence years. Finally, this study finds that there are dynamical differences leading to a systematic pattern of basin-wide warming following the El Niño-only years as compared to the IOD years. There is a systematic warming of the western Indian Ocean associated with the propagation of Rossby waves during the IOD years, and the surface heat fluxes play a more dominant role in leading the basin-wide warming following the peak of ENSO.

ACKNOWLEDGEMENTS

We thank the Director, IITM, and the Head of T.S. Division, IITM, for their support and encouragement. We acknowledge the Department of Ocean Development, Government of India, for the financial support through INCOIS: ISP (4.1): 2003. We also acknowledge NCEP/NCAR, BADC and UMD for various data sets used in this study. We thank Dr Emanuele Di Lorenzo, Georgia Institute of Technology, for providing the Matlab code, and for his suggestions to use the random composites to find the statistical significance and his many other suggestions that helped us to improve the manuscript considerably. We are also thankful to B. Thompson and A. Kulkarni for scientific discussions. The critical suggestions from an anonymous reviewer also helped us to improve the manuscript. Figures were prepared using GrADS and XMGRACE.

REFERENCES

Bjerknes J. 1969. Atmospheric teleconnections from the equatorial Pacific. *Monthly Weather Review* **97**: 163–172.

Bracco A, Kucharski F, Molteni F, Hazeleger W, Severijns C. 2005. Internal and forced modes of variability in the Indian Ocean. *Geophysical Research Letters* **32**: L12707, DOI: 10.1029/2005GL023154.

Carton JA, Chepurin G, Cao X, Giese B. 2000. A simple ocean data assimilation analysis of the global upper ocean 1950–95. Part I: methodology. *Journal of Physical Oceanography* **30**: 294–309.

Chambers DP, Tapley BD, Stewart RH. 1999. Anomalous arming in the Indian Ocean coincident with El Niño. *Journal of Geophysical Research* **104**: 3035–3047.

Chowdary JS, Gnanaseelan C, Vaid BH, Salvekar PS. 2006. Changing trends in the tropical Indian Ocean SST during La Nina years. *Geophysical Research Letters* **33**: L18610, DOI: 10.1029/2006GL026707.

Feng M, Meyers G. 2003. Interannual variability in the tropical Indian Ocean: a two-year time-scale of Indian Ocean Dipole. *Deep Sea Research Part II* **50**: 2263–2284.

Hareesh Kumar PV, Mathew B. 1997. On the heat budget of the Arabian Sea. *Meteorology and Atmospheric Physics* **62**: 215–224.

Kalnay E, Kanamitsu M, Kistler R, Collins W, Deaven D, Gandin L, Iredell M, Saha S, White G, Woollen J, Zhu Y, Chelliah M, Ebisuzaki W, Higgins W, Janowiak J, Mo KC, Ropelewski C, Wang J, Leetmaa A, Reynolds R, Jenne R, Joseph D. 1996. The NMC/NCAR 40-year reanalysis project. *Bulletin of the American Meteorological Society* **77**: 437–471.

Klein SA, Soden BJ, Lau NC. 1999. Remote sea surface temperature variations during ENSO: evidence for a tropical atmospheric bridge. *Journal of Climate* **12**: 917–932.

Lanzante JR. 1996. Lag relationships involving tropical SSTs. *Journal of Climate* **9**: 2568–2578.

Levitus S, Boyer TP. 1994. Temperature. *World Ocean Atlas 1994, NOAA Atlas NESDIS 4* **4**: 117.

Murtugudde R, McCreary JP, Busalacchi AJ. 2000. Oceanic processes associated with anomalous events in the Indian Ocean with relevance to 1997–1998. *Journal of Geophysical Research* **105**: 3295–3306.

Nicholson SE. 1997. An analysis of the ENSO signal in the tropical Atlantic and western Indian Oceans. *International Journal of Climatology* **17**: 345–375.

Prasad TG, McClean JL. 2004. Mechanisms for anomalous warming in the western Indian Ocean during dipole mode events. *Journal of Geophysical Research* **109**: C02019, DOI: 10.1029/2003JC001872.

Rao RR, Molinari RL, Festa JF. 1989. Evolution of the climatological near-surface thermal structure of the tropical Indian Ocean, 1, description of mean monthly mixed layer depth, sea surface temperature, surface current and surface meteorological fields. *Journal of Geophysical Research* **94**: 10,801–10,815.

Rao SA, Behra SK, Masumoto Y, Yamagata T. 2002. Interannual subsurface variability in the tropical Indian Ocean with a special emphasis on the Indian Ocean dipole. *Deep Sea Research Part II* **49**: 1549–1572.

Rayner NA, Parker DE, Horton EB, Folland CK, Alexander LV, Rowell DP, Kent EC, Kaplan A. 2003. Global analyses of sea surface temperature, sea ice, and night marine air temperature since the late nineteenth century. *Journal of Geophysical Research* **108**: D14,4407, DOI: 10.1029/2002JD002670.

Saji NH, Goswami BN, Vinayachandran PN, Yamagata T. 1999. A dipole mode in the tropical Indian Ocean. *Nature* **401**: 360–363.

Shenoi SSC, Shankar D, Shetye SR. 2002. Differences in heat budgets of the near-surface Arabian Sea and Bay of Bengal: during summer monsoon. *Journal of Geophysical Research* **107**: 3052, DOI: 10.1029/2001JC000679.

Shenoi SSC, Shankar D, Shetye SR. 2005. On the Accuracy of the Simple Ocean Data Assimilation analysis for estimating heat budgets of the near-surface Arabian Sea and Bay of Bengal. *Journal of Physical Oceanography* **35**: 395–400.

Tokinaga H, Tanimoto Y. 2004. Seasonal transition of SST anomalies in the Tropical Indian Ocean during El Niño and Indian Ocean Dipole Years. *Journal of the Meteorological Society of Japan* **82**(4): 1007–1018.

Tourre YM, White WB. 1997. Evolution of ENSO signals over the Indo-Pacific domain. *Journal of Physical Oceanography* **27**: 683–696.

Trenberth KE. 1997. The definition of El Niño. *Bulletin of the American Meteorological Society* **78**: 2771–2777.

Vinayachandran PN, Iizuka S, Yamagata T. 2002. Indian Ocean dipole mode events in an ocean General Circulation model. *Deep Sea Research Part II* **49**: 1573–1596.

Weare BC, Strub PT. 1981. The significance of sampling biases on calculated monthly mean oceanic surface heat fluxes. *Tellus* **33**: 211–224.

Webster PJ, Moore AM, Loschnigg JP, Leben RR. 1999. Coupled ocean-atmosphere dynamics n the Indian Ocean during 1997–1998. *Nature* **401**: 356–360.

Woodruff SD, Diaz HF, Elms JD, Worley SJ. 1998. COADS Release 2 data and metadata enhancements for improvements of marine surface flux fields. *Physics and Chemistry of the Earth* **23**: 517–526.

Wyrtki K. 1973. An equatorial jet in the Indian Ocean. *Science* **181**: 262–264.

Wyrtki K, Ulrich L. 1982. On the accuracy of heat storage computation. *Journal of Physical Oceanography* **12**: 1411–1416.

Yu L, Reinecker MM. 1999. Mechanism of the Indian Ocean warming during 1997–1998 El Niño. *Geophysical Research Letters* **26**: 735–738.

Zhang HM, Talley LD. 1998. Heat and buoyancy budgets and mixing rates in the upper thermocline of the Indian and Global Oceans. *Journal of Physical Oceanography* **28**: 1961–1978.